J. COMBIN. MATH. COMBIN. COMPUT. 127a (2025) 7721--7746

Journal of Combinatorial Mathematics and Combinatorial Computing
www.combinatorialpress.com/jcmcc

Combinatorial Press

Calculation of Fatigue Threshold and Crack Expansion Rate of Natural Gas Pressure Vessel Steels and Yield Strength Dependence Analysis

Gao Zhang[1,✉], Yajuan Wang[2], Junpeng Kang[1], Jia Li[3]

[1] *College of Architectural Surveying and Mapping, Shaanxi Energy Institute, Xianyang, Shaanxi, 712000, China*
[2] *College of Intelligent Mechatronics, Shaanxi Energy Institute, Xianyang, Shaanxi, 712000, China*
[3] *School of Construction Machinery, Chang'an University, Xi'an, Shaanxi, 710064, China*

ABSTRACT

In this paper, the strain law of natural gas pressure vessel steel fatigue is firstly analyzed through the stress-strain curve and steel fatigue life curve, and the finite element model of natural gas pressure vessel is constructed by combining ABAQUS simulation software, and the fatigue performance of natural gas pressure vessel steel is analyzed from the cyclic softening behavior of the material and S-N curve. Then the stress intensity factor theory combined with Paris formula is introduced to calculate the crack expansion rate, and ABAQUS and FTANC3D are jointly simulated to study the crack expansion law. Finally, the fatigue yield strength of the natural gas pressure vessel was analyzed based on the elastic-viscoplastic constitutive model combined with the finite element model. It is found that the stress intensity factor along the path under hydrostatic loading is larger than that under stress-containing loading, but the difference in stress intensity factor is only about 1.42%. When the cracks of the natural gas pressure vessel extended to the vicinity of 20 mm, its crack extension rate showed a sharp downward trend. When the temperature comes to 900°C, the yield strength value of the steel of natural gas pressure vessel is only 280.42 MPa.Exploring the steel fatigue performance and crack extension rate of natural gas pressure vessel can help to better ensure the stable and safe operation of natural gas pressure vessel.

Keywords: stress-strain curve, S-N curve, stress intensity factor, Paris formula, elastic-viscoplastic constitutive model, crack extension rate

✉ Corresponding author.
E-mail address: sanhu1989hugh@163.com (G. Zhang).
Received 25 March 2024; Revised 05 June 2024; Accepted 15 December 2024; Published Online 15 April 2025.
DOI: 10.61091/jcmcc127a-427

1. Introduction

Natural gas is a high-quality, high-efficiency and clean new energy in this century, which has attracted much attention from countries all over the world for its energy-saving, environmentally friendly, economic and convenient advantages. It can be used as a fuel in industrial and agricultural production and people's life, as a chemical raw material, and as a fuel for automobiles, air conditioners and so on [1-3]. This has brought benefits in various aspects such as improving economic efficiency, reducing urban air pollution and facilitating residents' life, but the ensuing various safety problems have also brought deep worries to people. Among the many safety problems of natural gas, the safety of pressure vessels is undoubtedly an important part. Pressure vessel involves life safety, danger, once the accident will not only bring personal injury and property loss, and even seriously affect social stability [4].

Pressure vessel is an indispensable equipment in the process of industrial production, which is widely used in oil refining, machinery, textile, metallurgy, nuclear energy and transportation and other national economic sectors. Because it holds flammable, explosive, toxic or corrosive media and is subjected to high temperature and high pressure for a long time, the pressure vessel is a special equipment with high danger in the industrial production process [5]. When the vessel is pressurized, the material will undergo stress concentration and deformation due to the high pressure of the internal medium. With the change of pressure, this stress concentration and deformation will occur repeatedly, making the material gradually fatigue under such alternating stresses, which eventually leads to fatigue damage [6-7]. Therefore, its materials must have excellent mechanical properties and strength. However, fatigue damage is different from other damage modes, which is not easy to be found in daily inspection and triggers sudden accidents, and even the best materials are susceptible to deformation and fatigue during prolonged use, which can greatly threaten production safety and work efficiency [8-9]. In addition, the long-term use of pressure vessels, changes in material properties, the corrosive effect of the medium will lead to cracks in the vessel wall, which may lead to serious accidents [10-12]. The static crack extension is mainly affected by factors such as stress level and stress concentration, while the fatigue crack extension is gradually expanded under cyclic loading [13-14]. As a result, factors such as the material, medium, and operating conditions of the pressure vessel will have an impact on crack extension. Among them, the material properties will determine the rate and path of crack expansion, the corrosiveness of the medium will exacerbate the degree of crack expansion, and the working conditions, such as temperature and pressure, will increase the brittleness of the material will also have an impact on crack expansion [15-18]. It is therefore potentially very harmful and should be given high priority by equipment managers.

Fatigue threshold is a characterization of the crack extension resistance of a material or structure under fatigue loading, which is one of the important indicators for evaluating the fatigue resistance of a material, and accurately determining the fatigue threshold can help us to evaluate the safety of the structure, and develop reasonable maintenance and inspection strategies [19]. Crack extension rate is the rate of crack tip expansion from the early stage of crack development to the expansion [20]. Both are important parameters for predicting and controlling the fatigue life of a material or structure. Yield strength is the lowest value of stress at which a material begins to undergo significant plastic deformation and has a significant effect on the fatigue performance and crack extension of the material [21-23]. Therefore, it is of great significance to analyze the interrelationship between yield strength and the two by calculating the fatigue threshold value and crack extension rate of a natural gas pressure vessel made of steel, for the improvement of the safety of natural gas pressure vessels.

In order to explore the performance of natural gas pressure vessel, data simulation is carried out in three dimensions, namely, steel fatigue, crack extension rate and yield strength. In the analysis of steel fatigue performance, a finite element model is established by using the stress-strain curve combined with ABAQUS simulation software to analyze the cyclic softening behavior of the material and the trend of S-N curve. In the crack extension rate calculation, it is based on the stress intensity factor theory and Paris formula, and the crack extension law is analyzed by the joint simulation of ABAQUS and FTANC3D. Finally, based on the elastic-viscoplastic intrinsic model and finite element model, the specific effects of loading rate and temperature on the fatigue yield strength of natural gas pressure vessel steel are analyzed.

2. Calculation of fatigue thresholds for natural gas pressure vessel steels

Natural gas pressure vessels have been in service for a long time, and the proportion of defective natural gas pressure vessels is increasing. Steel fatigue reliability analysis of existing defective natural gas pressure vessels can better ensure the safe operation of natural gas pressure vessels. Based on this, exploring the steel fatigue strain of natural gas pressure vessels and analyzing their steel fatigue service life is an important method for using units to ensure the stable operation of natural gas pressure vessels.

2.1. Fatigue strain law of pressure vessel steel

2.1.1. Stress-strain relationship. Natural gas pressure vessel equipment in the work situation, will be subject to changes in temperature due to working conditions, intermittent operation, operation process fluctuations and the constant changes in the load applied to it, so that the natural gas pressure vessel equipment to withstand the repeated action of the alternating load, in the long term, some of the structure or components of the equipment will occur fatigue damage. Since the natural gas pressure vessel is made of special steel plates for pressure vessels, the alternating loads it is subjected to in the course of its work and the environmental conditions in which it is located cause its fatigue damage to fall into the category of low-week fatigue. A study of the strain fatigue performance of the components of a natural gas pressure vessel will provide a true picture of the fatigue life development of the pressure vessel. The most basic parameter used for strain fatigue life analysis is the strain fatigue property of the material, which is a very important indicator for describing the fatigue characteristics of metallic materials. The relationship between stress and strain of a metal material in tension and compression is the most basic relationship reflecting its performance.

Taking the uniaxial static tensile test of a standard specimen material as an example, the specimen material is elongated axially and necked transversely after stretching. During the homogeneous deformation process before transverse necking, unloading at any point on the $\sigma-\varepsilon$ curve, its elastic strain ε_e can be recovered; and its plastic strain ε_p is left as residual deformation [24].

The strain ε at each point on the stress-strain curve is the sum of its elastic, and plastic strains, i.e:

$$\varepsilon = \varepsilon_e + \varepsilon_p \tag{1}$$

The relationship between stress and elastic strain of a material satisfies Hooke's theorem with the relation:

$$\sigma = E\varepsilon_e \tag{2}$$

The relationship between stress and plastic strain of a material satisfies Solomon's theorem, which is given by:

$$\sigma = K\left(\varepsilon_p\right)^n \tag{3}$$

Combining the above equations (2) and (3) gives the Remberg-Osgood stress versus its elastic-plastic strain as:

$$\varepsilon = \varepsilon_e + \varepsilon_p = \frac{\sigma}{E} + \left(\frac{\sigma}{K}\right)^n \tag{4}$$

where k for the strength coefficient, n for the material strain hardening index, when $n = 0$, that is to say that the material does not occur strain hardening, the material stress and plastic strain has no relationship between the material, that is, the material for the ideal plastic material.

The strain fatigue performance of the metal material is to reflect the relationship between the strain of the material and its fatigue life, that is, with $\varepsilon - N$ curve to describe. The fatigue life test is performed by the standard fatigue test method, where a fatigue test with symmetrical cycles at a constant strain amplitude is implemented at stress ratio $R = -1$. Wherein, during each strain cycle loading, there are two reversals, so the fatigue life is expressed in terms of the number of load reversals $2N$, where N is the number of load cycles. The smaller the strain amplitude ε_a, the longer the fatigue life N of the mechanical part or component.

In the long-life region, mainly elastic strain ε_{pa} dominates, and the effect of plastic strain part ε_{ea} can be neglected, $\varepsilon_a \approx \varepsilon_{ea}$, and:

$$\varepsilon_{pa} = \varepsilon_f'(2N)^c \ Or \ \varepsilon_{pa}^{m_2} N = C_2 \tag{5}$$

The above equation is the well-known Mason-Coffin low-week strain fatigue equation.

$\varepsilon - N$ curve of a metallic material tested by fatigue under the control of strain load. At strain amplitude $\varepsilon_a = 0.01$, the fatigue life of most materials is the same. In the region of high strain, low life, the ductility of the metal material determines whether its fatigue life increases; while in the region of low strain, high life, the strength of the material, the longer its life.

2.1.2. Steel fatigue life curves. Fatigue failure before the number of cycles of stress or strain is called fatigue life, the fatigue life of the specimen depends on the mechanical properties of the material and the level of applied stress, in general, the higher the limit of the strength of the material, the lower the level of applied stress, the fatigue life of the specimen the longer, and vice versa, the shorter the fatigue life. Indicates the relationship between this applied stress level and the fatigue life of the standard specimen curve is called the S-N curve of the material.

S-N curve of the left section in double logarithmic coordinates is generally a straight line, in single logarithmic coordinates is generally not a straight line, but due to the simplicity of using a straight line to express the single logarithmic coordinates are often simplified to a straight line. S-N curve of the right section can be divided into two types, the first type is a clear level of the section for the structural steel and titanium alloys of the typical form, the second type does not have the level of the section is a typical form of non-ferrous metals and corrosion fatigue. The second type has no horizontal segment and is typical of non-ferrous metals and corrosion fatigue.

$S - N$ The left segment of a curve is often expressed by an equation of the following form:

$$\sigma^m N = C \tag{6}$$

where m and C are material constants. Taking the logarithm of both sides of the above equation gives:

$$m \lg \sigma + \lg N = \lg C \tag{7}$$

It can be seen that the above equation is equivalent to the left segment of the $S - N$ curve being a straight line in double logarithmic coordinates and $1/m$ being the negative slope of the $S - N$ curve. It is also common to represent the entire $S - N$-curve by the following equation, viz:

$$(\sigma - A)^m N = D \tag{8}$$

Or:

$$\sigma = A\left(1+\frac{C}{N^{a}}\right) \tag{9}$$

where $1/m$ is the negative slope of the $S-N$ curve, the fatigue limit of the material, D is the material constant, α is the negative slope of the $S-N$ curve, and C is the material constant.

2.2. Pressure vessel finite element modeling

2.2.1. ABAQUS simulation software. In this study, ABAQUS finite element software was used to simulate steel materials for natural gas pressure vessels with the aim of investigating their failure fracture in tension and fatigue life.

ABAQUS is an advanced engineering simulation and analysis software widely used for solving a wide range of complex problems in engineering, including structural strength analysis, heat transfer, fluid dynamics, and multi-physics field coupling. It provides a rich set of material models, element types, and analytical capabilities to accurately simulate physical behavior from micro to macro scales [25]. The power of the ABAQUS software lies in its flexible modeling capabilities and accurate solvers, which enable it to handle complex situations including nonlinearities, large deformations, and contact problems.

For the natural gas pressure vessel steel material in this study, ABAQUS was able to simulate the stress-strain response of the material during tension, which in turn predicted the point of fatigue in the steel, analyzed the crack extension paths, and evaluated the fracture toughness of the material. And the post-processing tools of ABAQUS can also provide intuitive graphical outputs, such as stress distribution, dynamic demonstration of the steel fatigue process, etc., which provides an intuitive perspective for understanding the steel fatigue of the material.

2.2.2. Modeling and Boundary Conditions. A finite element model of the natural gas pressure vessel containing an elliptical shallow cracked cylinder on the inner surface is established. Since the natural gas pressure vessel is subjected to various types of loads, the pressure vessel vibrates, so the action of the medium inside the vessel on the inner wall is not continuous. The temperature of the natural gas inside the pressure vessel is also changing along the direction of the wall thickness, and there are temperature difference stresses. The inner wall of the cylinder is subjected to the role of tensile stress caused by the working internal pressure, but also subjected to the role of the tensile pressure generated by the temperature difference, the superposition of the two kinds of tensile stress, so that the inner wall of the stress reached its maximum value. Therefore, the thermal coupling analysis in ABAQUS software is used to calculate the fatigue life.

For the solid, when modeling, the units usually used are Solid40, Solid90, Solid95, Solid180, Solid185 these units. The unit selected in this chapter is the 12-node tetrahedral unit (Solid180). Since the pressure vessel is an irregular model, the Solid180 cell is a high-order 3D 12-node solid structural cell with a quadratic displacement model, which has advantages over other cells in simulating irregular models. The cell is characterized by plasticity, hyperelasticity, creep, large deformation and large strain. Considering the calculation volume and accuracy, the mesh type used in this paper is tetrahedral mesh, and the size of the selected mesh is 12 mm.The calculation object is transformed into a mechanical model, and a part of the cylinder with cracks is taken as the research object to establish a mechanical model. There are 331678 nodes and 246592 cells in the model.

The design pressure of the vessel is 1.5 MPa, loaded on the inner wall of the cylinder. The temperature of the crude oil inside the vessel fluctuates between 45°C and 70°C, and the minimum temperature of the external environment is -10°C. An insulation layer needs to be applied to the outer wall of the cylinder, so the temperature load also needs to be considered. After setting the temperature load in the analysis setup and loading it, the impact force of the natural gas in the vessel on the inner wall is constantly changing during the loading process, as well as the temperature of the outer wall and the temperature of the inner wall, which causes fatigue in a certain period of time.

In order to restore the situation of the real constraint force, so the symmetric constraint is applied on the symmetric surface, and in order to ensure that there is no axial movement of the natural gas pressure vessel, the axial homobrachial force of equal size and opposite direction is applied on the two sections of the pressure vessel. Its calculation formula can be expressed as:

$$P_c = \frac{PD_i^2}{\left(D_i + 2t\right)^2 - D_i^2} \tag{10}$$

where P is the internal pressure, D_i is the inner diameter of the cylinder, and t is the thickness of the cylinder.

2.3. Fatigue Performance Analysis of Pressure Vessel Steels

2.3.1. Cyclic softening behavior of materials. During low-cycle fatigue experiments, the initial stress-strain curves are not completely closed due to the response of the material to cyclic loading. The characteristic curve of cyclic response obtained through the maximum and minimum stresses of each cycle is particularly important for analyzing the cyclic behavior of the material. The strain-controlled cyclic response characteristic curve of natural gas pressure vessel steel material is shown in Fig. 1. Among them, Fig. 1(a)~(b) shows the cyclic response characteristic curves at room temperature and high temperature, respectively.

From the perspective of the whole fatigue life, the cyclic response characteristic curves of the material at different temperatures show a continuous decreasing trend, i.e., a continuous softening phenomenon. Comparing Fig. 1(a) and (b), it can be seen that the higher the temperature, the lower the stress amplitude of the material in the case of the same strain amplitude. At the same time, the higher the strain amplitude, the higher the stress amplitude of the material for the same temperature. Therefore, temperature and strain amplitude can affect the cyclic softening behavior of natural gas pressure vessel steel fatigue.

In addition, the cyclic response characteristic curve of the material at different temperatures can be divided into three parts. First, the cyclic softening phenomenon is particularly obvious in phase Ⅰ of the cyclic response characteristic curve, i.e., the first 15% of the fatigue life, and the fatigue performance of the material degrades with the crack initiation. Immediately after the cyclic response characteristic curve into the Ⅱ stage, that is, the fatigue life of 15% to 75% of the cyclic softening between the stable decline in the area, the value of the stress shows a slow decline in the trend, at this time, the crack into a stable expansion stage. When the fatigue life reaches 75%, i.e. stage III, the cyclic response characteristic curve of the material decreases rapidly and eventually fails. However, under high temperature environment, due to the severe necking of the specimen and the influence of cyclic softening, the cyclic response characteristic curve starts to decrease rapidly in the region of 65% of the fatigue life, and the cyclic response characteristic curve with the strain amplitude of 1.5% changes most obviously. The above results indicate that the influence of temperature on the material properties of natural gas pressure vessel steels is crucial, which controls the cyclic softening behavior of the materials.

At room temperature, the hysteresis curves for fatigue life up to 75% of the fatigue life showed only slight changes, while the hysteresis curves for fatigue life after 75% showed large differences, which indicates that the material has stable fatigue properties when the cracks are steadily expanding, and severe fatigue property degradation does not occur until after 75% of the fatigue life. On the contrary, of all the hysteresis curves of strain amplitude for high temperature environments, the hysteresis curves change significantly below 75% of the fatigue life, after which the fatigue behavior develops steadily until failure. Therefore, temperature is an important factor influencing the hysteresis curve change and low week fatigue performance. At the same time, the fatigue life of a material can also be controlled by temperature.

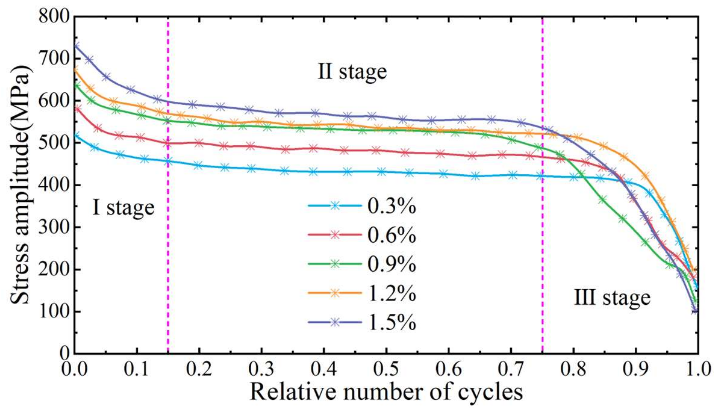

(a) Normal temperature

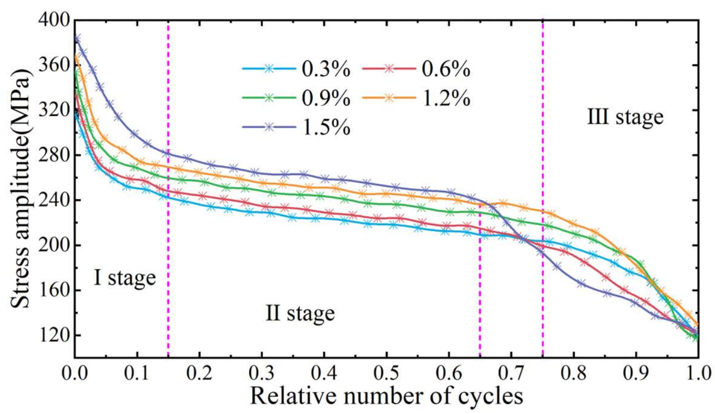

(b) High temperature

Fig. 1. Cyclic response characteristic curve

2.3.2. Trends in S-N curves. In order to study the fatigue performance of natural gas pressure vessels in different environments, fatigue tests were carried out by a rotary bending fatigue testing machine based on the finite element model designed in the previous section, the loading frequency was 30~35 Hz, respectively, the stress ratio was set to -0.5, and the fatigue limit was determined by the lift-off method. According to the existing standards, the test is stopped when the specimen fails or the loading number reaches 10^7 cycles (in air) or 2×10^7 cycles (in corrosive environment). The S-N curves of the fatigue performance of natural gas pressure vessel steels in different environments are shown in Fig. 2.

For all specimens, the fatigue life increased as the stress level decreased. The fatigue test results show that the fatigue limit of 323.78 MPa exists for the specimens in the air environment within 10^7 cycle cycles, whereas in the corrosive environment, the specimens do not have a fatigue limit within 10^7 cycle cycles, and the fatigue strength corresponding to 10^7 cycle cycles decreases to 148.97 MPa, which is an overall 53.99% reduction in the fatigue life of the natural gas pressure vessel steel compared to that of the natural gas pressure vessel steel in the air environment. In the high stress (more than 323.78MPa, relative to the fatigue limit in the corrosive environment) loading, the fatigue life in the corrosive environment and the fatigue life in the air environment are very similar, which indicates that in the case of high stress, the corrosive environment does not have much influence on the fatigue life, and at this time the fatigue life is mainly controlled by the loading stress. The fatigue strength of the specimens in the corrosive environment was significantly reduced when the loading stress was lower than 323.78 MPa. This indicates that the corrosive environment significantly reduces the fatigue performance of the specimens at stress levels lower than the fatigue limit in the air environment. It can be seen that the steel fatigue life thresholds of natural gas pressure vessels in different environments are 323.78 MPa and 148.97 MPa in air and corrosive environments, respectively, which provide some data support for optimizing the safety preservation of natural gas pressure vessels.

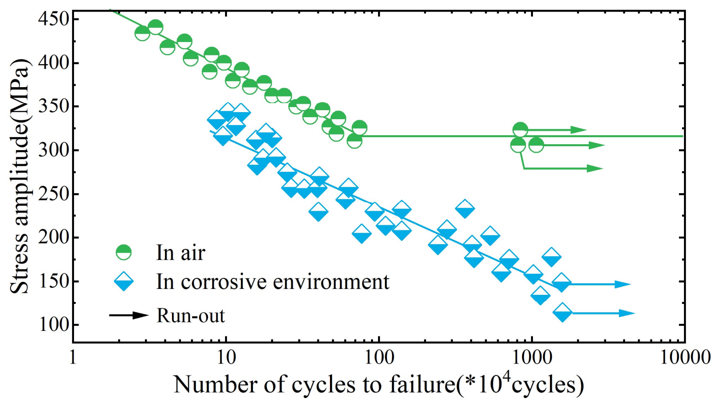

Fig. 2. Steel fatigue performance S-N curve

3. Calculation of crack propagation rate in natural gas pressure vessels

Under the premise of the "14th Five-Year Plan" and the "Double Carbon" target, natural gas, as a clean and low-carbon energy source, will be used as the main alternative to traditional high-carbon fossil energy sources. Cracks are the most hazardous defects often found in the inspection of natural gas pressure vessels in service, but in the actual use of natural gas pressure vessels there will inevitably be the original, nascent crack defects. When crack defects are found during the regular inspection of in-service pressure vessels, the user unit may not be able to deal with the crack defects found during the inspection immediately because of the continuous production or the cycle of guaranteeing the supply of natural gas. Therefore, the safety evaluation of crack defects to ensure the safe operation of natural gas pressure vessels has become an inevitable demand of the user units.

3.1. Influencing factors and laws of crack extension

3.1.1. Stress intensity factor theory. The local or overall destruction of a material or component under the action of load is called fracture, and cracking is the main cause of fracture in macroscopic materials. In fracture mechanics, cracks are classified into different types under different classification criteria in order to systematically study the characteristics of cracks [26]. According to the cracking force characteristics, the cracks can be divided into three basic types, which are called open (type I), slip open (type II), and tear open (type III) cracks, and the basic forms of cracks are shown in Figure 3. Type I cracks are subject to tensile stresses perpendicular to the crack face. Type II cracks are subjected to shear stresses parallel to the crack face but perpendicular to the leading edge of the crack. Type III cracks are subjected to shear stresses parallel to both the crack face and the crack leading edge. Type I cracks are the most common of the above three types of cracks, and type I cracks are the most likely to produce low-stress brittle fracture, which has serious implications, but in practice they are mostly composite cracks.

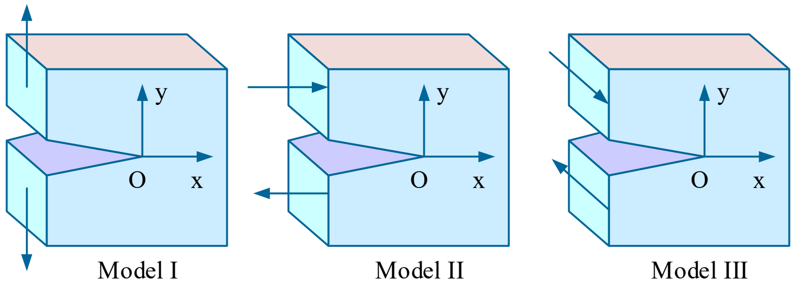

Fig. 3. The basic form of crack

In the field of linear elasticity, to solve the stress function for a crack tip type I crack, the stress function $U(x, y)$ must satisfy the coordination equation, i.e.:

$$\nabla^4 U = 0 \tag{11}$$

The crack tip is the origin of a right-angle coordinate system, with axis X parallel to the crack and axis Y perpendicular to the crack. On the crack surface, the surface force is zero, then:

$$\sigma_\theta = \tau_{r\theta} = 0 \theta = \pm\pi \tag{12}$$

where σ_θ and $\tau_{r\theta}$ are the circumferential positive and shear stresses in the polar coordinate system, respectively.

To discuss the singular field near the crack tip, it is assumed that the stress function U can be expressed in the form of separated variables as:

$$U(r,\theta) = r^{1+\lambda} F_\lambda(\theta) \tag{13}$$

Substituting Eq. (13) into Eq. (11), the equation about F_i is obtained as:

$$F_\lambda'''(\theta) + 2\left(\lambda^2+1\right)F_\lambda''(\theta) + \left(\lambda^2-1\right)^2 F_\lambda(\theta) = 0 \tag{14}$$

The generalized solution of this equation is:

$$\begin{aligned} F_\lambda(\theta) = {} & A\cos(\lambda+1)\theta + B\sin(\lambda+1)\theta \\ & + C\cos(\lambda-1)\theta + D\sin(\lambda-1)\theta \end{aligned} \tag{15}$$

The components in the polar coordinate system are:

$$\begin{cases} \sigma_r = \dfrac{1}{r^2}\dfrac{\partial^2 U}{\partial\theta^2} + \dfrac{1}{r}\dfrac{\partial U}{\partial\theta} = r^{\lambda-1}\left[F_\lambda'' + (\lambda+1)F_\lambda\right] \\ \sigma_\theta = \dfrac{\partial^2 U}{\partial r^2} = r^{\lambda-1}\lambda(\lambda+1)F_\lambda \\ \tau_{r\theta} = -\dfrac{\partial}{\partial r}\left(\dfrac{1}{r}\dfrac{\partial U}{\partial r}\right) = r^{\lambda-1}\lambda F_\lambda' \end{cases} \tag{16}$$

Substituting Eq. (16) into Eqs. (12) and (11) yields the stress function U which is the Williams stress function, and the expression for the stress component of the cracked body in polar coordinates is obtained by using the method of separated variables:

$$\sigma_r = \sum_{n=1}^{\infty} \frac{n}{2} C_n r^{\frac{n}{2}-1} \left\{ \left[\frac{n}{2} + (-1)^n \right] \cos\left(\frac{n}{2}+1 \right)\theta - \left(\frac{n}{2}-3 \right) \cos\left(\frac{n}{2}-1 \right)\theta \right\}$$
$$+ \sum_{n=1}^{\infty} \frac{n}{2} D_n r^{\frac{n}{2}-1} \left\{ \left[\frac{n}{2} - (-1)^n \right] \sin\left(\frac{n}{2}+1 \right)\theta - \left(\frac{n}{2}-3 \right) \sin\left(\frac{n}{2}-1 \right)\theta \right\} \tag{17}$$

$$\sigma_\theta = \sum_{n=1}^{\infty} \frac{n}{2} C_n r^{\frac{n}{2}-1} \left\{ -\left[\frac{n}{2} + (-1)^n \right] \cos\left(\frac{n}{2}+1 \right)\theta + \left(\frac{n}{2}+1 \right) \cos\left(\frac{n}{2}-1 \right)\theta \right\}$$
$$+ \sum_{n=1}^{\infty} \frac{n}{2} D_n r^{\frac{n}{2}-1} \left\{ -\left[\frac{n}{2} - (-1)^n \right] \sin\left(\frac{n}{2}+1 \right)\theta + \left(\frac{n}{2}+1 \right) \sin\left(\frac{n}{2}-1 \right)\theta \right\} \tag{18}$$

$$\sigma_{r\theta} = -\sum_{n=1}^{\infty} \frac{n}{2} C_n r^{\frac{n}{2}-1} \left\{ \left[\frac{n}{2} + (-1)^n \right] \sin\left(\frac{n}{2}+1 \right)\theta - \left(\frac{n}{2}+1 \right) \sin\left(\frac{n}{2}-1 \right)\theta \right\}$$
$$- \sum_{n=1}^{\infty} \frac{n}{2} D_n r^{4-1} \left\{ -\left[\frac{n}{2} - (-1)^n \right] \cos\left(\frac{n}{2}+1 \right)\theta - \left(\frac{n}{2}+1 \right) \cos\left(\frac{n}{2}-1 \right)\theta \right\} \tag{19}$$

Eqs. (17), (18) and (19) are expressions for the crack tip stresses, which result mainly from the first term, and the remaining terms can be neglected. The result is mainly the first term, and the rest of the terms can be neglected. $n = 1$, $K_I = C_1\sqrt{2\pi}$, $K_{II} = D_1\sqrt{2\pi}$ in Eqs. (17), (18) and (19). The type I crack produces only open-type fracture, i.e., $K_I \neq 0$, $K_{II} = 0$, when the bi-directional homogeneous tensile load is applied, and substituting K_I and K_{II} into Eqs. (17), (18) and (19), the deduced stress-strain field of the crack tip of the type I crack in the right-angled coordinate system can be expressed as follows:

$$\begin{cases} \sigma_x = \dfrac{K_I}{\sqrt{2\pi r}} \cos\dfrac{\theta}{2}\left(1 - \sin\dfrac{\theta}{2} \sin\dfrac{3\theta}{2} \right) \\ \sigma_y = \dfrac{K_I}{\sqrt{2\pi r}} \cos\dfrac{\theta}{2}\left(1 + \sin\dfrac{\theta}{2} \sin\dfrac{3\theta}{2} \right) \\ \tau_{xy} = \dfrac{K_I}{\sqrt{2\pi r}} \sin\dfrac{\theta}{2} \cos\dfrac{\theta}{2} \cos\dfrac{3\theta}{2} \\ u_x = \dfrac{K_I}{2G}\sqrt{\dfrac{r}{2\pi}} \cos\dfrac{\theta}{2}\left(\kappa - 1 + 2\sin^2\dfrac{\theta}{2} \right) \\ u_y = \dfrac{K_I}{2G}\sqrt{\dfrac{r}{2\pi}} \sin\dfrac{\theta}{2}\left(\kappa + 1 - 2\cos^2\dfrac{\theta}{2} \right) \end{cases} \tag{20}$$

Type II crack is under the action of uniform shear stress, at this time $K_I = 0$, $K_{II} \neq 0$, according to the stress rotational axis formula, the stress-strain field at the tip of the type II crack under the right-angle coordinate system is obtained can be expressed as:

$$\begin{cases} \sigma_x = \dfrac{K_H}{\sqrt{2\pi r}} \sin\dfrac{\theta}{2}\left(2+\cos\dfrac{\theta}{2}\cos\dfrac{3\theta}{2}\right) \\ \sigma_y = \dfrac{K_H}{\sqrt{2\pi r}} \sin\dfrac{\theta}{2}\cos\dfrac{\theta}{2}\cos\dfrac{3\theta}{2} \\ \sigma_{xy} = \dfrac{K_H}{\sqrt{2\pi r}} \cos\dfrac{\theta}{2}\left(1-\sin\dfrac{\theta}{2}\sin\dfrac{3\theta}{2}\right) \\ u_x = \dfrac{K_H}{2G}\sqrt{\dfrac{r}{2\pi}} \sin\dfrac{\theta}{2}\left(\kappa+1+2\cos^2\dfrac{\theta}{2}\right) \\ u_y = \dfrac{K_H}{2G}\sqrt{\dfrac{r}{2\pi}} \cos\dfrac{\theta}{2}\left(\kappa-1-2\sin^2\dfrac{\theta}{2}\right) \end{cases} \tag{21}$$

where, r is the stress intensity factor control radius at the crack tip, θ is the azimuthal angle in the region centered on the crack tip, G is the shear modulus of the material, and κ is the elastic constant of the material, which is related to the Poisson's ratio of the material v as follows:

$$\kappa = \begin{cases} 3-4v, \text{ Plane Strain} \\ \dfrac{3-v}{1+v}, \text{ Plane Stress} \end{cases} \tag{22}$$

3.1.2. Calculation of crack propagation rate. Regarding the crack expansion rate of natural gas pressure vessel, the solution path mainly includes determining the crack expansion rate and crack expansion direction. Fig. 4 shows the crack expansion stages of natural gas pressure vessel, which are crack initiation, stable crack expansion and rapid fracture.

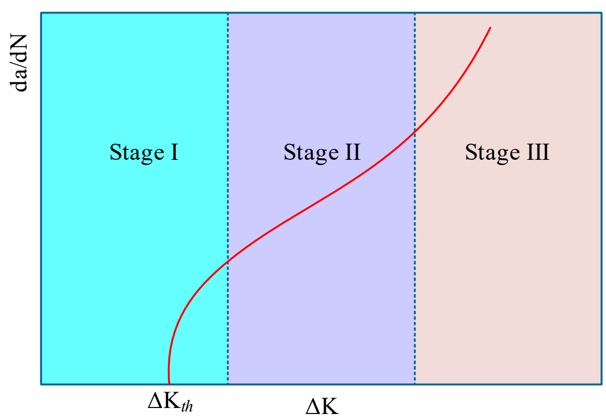

Fig. 4. Crack extension of pressure vessel

The first stage is the initial expansion of the crack, the figure can be seen in stage I there is a threshold value, before the threshold value has not yet begun to produce cracks, with the continuous cyclic application of stress, the stress intensity factor amplitude across this threshold, cracks begin to appear. The second stage is the stable crack expansion stage, which is the main stage of crack expansion and can be expressed by the Paris formula. The third stage is the rapid crack expansion stage, at this time the crack expansion rate has basically reached the maximum expansion rate, so in this stage, the crack will be rapidly expanded, and at this time the material is close to the fracture toughness, the material is about to fail. This stage will be in a very short period of crack expansion to the critical size, the material will quickly reach the failure conditions. Considering that in practice, the life cycle of metallic materials is long, so the cycle time of the rapid crack expansion phase is only a small part of the whole life cycle, and the cycle time of this phase is not considered to be of great influence [27].

The mathematical form of Paris formula is expressed as:

$$\frac{da}{dN} = C(\Delta K)^m \tag{23}$$

where a is the crack length, N is the number of stress cycles (fatigue extension life), da/dN is the crack extension rate, C and m are material-related constants called coefficients and indices, respectively, and ΔK is the stress intensity factor amplitude.

The critical crack length a_c is obtained from the linear elastic fracture mechanics criterion:

$$\Delta K = K_{\max} - K_{\min} = f\Delta\sigma\sqrt{\pi a} \tag{24}$$

Ditto:

$$a_c = \frac{(K_{\max}/f\sigma)^2}{\pi} \tag{25}$$

where $K_{\max}$ is the maximum value of the stress intensity factor, $K_{\min}$ is the minimum value of the stress intensity factor, f is a function related to the dimensions of a and W, which can be obtained by consulting the manual, and $\Delta\sigma$ is the stress amplitude at the crack.

The linear superposition model indicates that the crack extension of the natural gas pressure vessel is subject to the synergistic effect of the environment and the alternating load, so that the fatigue crack extension rate and the stress crack extension rate can be added, and the sum of the two is the crack extension rate. Then:

$$\left(\frac{da}{dN}\right)_{CF} = \left(\frac{da}{dN}\right)_F + \left(\frac{da}{dN}\right)_{SCC} \tag{26}$$

where $(da/dN)_{CF}$ is the fatigue crack extension rate after superposition, $(da/dN)_F$ is the fatigue crack extension rate for mechanical loading, and $(da/dN)_{SCC}$ is the stress crack extension rate.

If the effect of the time factor on the stress crack expansion rate is taken into account and τ is the cycle period, there is:

$$\left(\frac{da}{dN}\right)_{SCC} = \int \tau \left(\frac{da}{dt}\right)_{SCC} dt \tag{27}$$

If Eq. (26) is expressed in the form of crack expansion per unit time, we have:

$$\left(\frac{da}{dt}\right)_{CF} = f\left(\frac{da}{dt}\right)_F + \left(\frac{da}{dt}\right)_{SCC} \tag{28}$$

Typically, at higher loading frequencies f, fatigue crack propagation plays a major role, while at lower loading frequencies f, stress crack propagation plays a major role.

3.1.3. Change rule of crack expansion. In the Paris zone, the crack extension rate can be expressed by the Paris equation as:

$$da/dN = C(\Delta k)^m \tag{29}$$

where d for the differential, a for the size of the crack, N for the number of stress cycles, C, m is related to the material properties of the constant.

From the above equation, it can be seen that the expansion rate of the pressure vessel and the crack size and the number of stress cycles, through the above equation can be obtained dN, on the dN ends of the integral can be obtained:

$$N = \int_0^N \frac{da}{C(\Delta k)^m} \tag{30}$$

Let the crack sizes be a_0 and a_N for stress cycle numbers 0 and N. If crack size a_N corresponds exactly to the rate inflection point, the number of cycles required for the crack to go from a_0 to a_N is the remaining life, and thus the remaining life prediction problem can be converted to a problem of how to determine a_N. The crack depth a and length l are calculated iteratively using the Paris formula to obtain:

$$da / dN = C\left(\Delta k^a\right)^m \tag{31}$$

$$dl / dN = C\left(\Delta k^l\right)^m \tag{32}$$

where Δk^a and Δk^l are the range of variation of stress intensity factor at depth a and length l, respectively.

The range of variation of the crack stress intensity factor determines the depth and length of the crack. Let the initial depth of the crack be a_0 and the initial length be l_0, and each time the crack length increases by an infinitesimal amount Δl, the change in depth Δa is:

$$\Delta a = \left(\Delta k^{a_0} / \Delta k^{l_0}\right)^m \Delta l \tag{33}$$

Therefore, when the crack changes n time, the length l_n and depth a_n of the crack are respectively:

$$l_n = l_{n-1} + \Delta l \tag{34}$$

$$a_n = a_{n-1} + \left(\Delta k^{a_{n-1}} / \Delta k^{l_{n-1}}\right)^m \Delta l \tag{35}$$

The dimensions of cracks include length, depth and width, the crack depth has the greatest influence on the safety of natural gas pressure vessels, followed by length, and the crack width does not directly affect the safety, but indirectly through the depth and length. From the above equation, it can be seen that the length of the crack increases linearly, but the depth of the crack increases nonlinearly, and the changes of the crack length and depth need to be considered simultaneously when calculating the remaining life.

3.2. Crack Expansion Simulation of Pressure Vessels

3.2.1. FTANC3D Simulation Software. FTANC3D is a set of fracture analysis software dedicated to the simulation study of crack extension of engineering components, whose functions include simple modeling, calculating stress intensity factor, and setting the automatic extension of cracks. Adopting FTANC3D software to the crack extension law of natural gas pressure vessel has high professionalism, and it can simulate the structure of any complex shape, set the load and boundary conditions arbitrarily. It is suitable for the actual engineering structure, and the fatigue crack extension law and the fatigue life of the cracks obtained through simulation calculation have high credibility.

FTANC3D software consists of the following three parts:

1) Stereo object modeler. It is equivalent to the pre-processing module, but can only construct simple geometric models and generally describe the objects that can be imported into FTANC3D.

2) Fracture Analyzer. The simulated crack extension capability is powerful, and the software comes with a crack library, so that you can arbitrarily select the crack type according to the experimental requirements, such as circular cracks, linear cracks, and so on. When the required crack type is more complex, the crack body can also be constructed manually.

3) Boundary element system. It mainly deals with the problems imposed by boundary conditions and material parameters. In terms of mesh division, the model mesh can be divided automatically along with the crack expansion process, which is an advantage that other 3D simulation software does not have.

3.2.2. Initial conditions for numerical simulation. In order to deeply analyze the crack extension efficiency of the natural gas pressure vessel, this paper combines the ABAQUS software given in the previous section with FTANC3D for joint simulation. The joint simulation flow of crack extension of natural gas pressure vessel based on ABAQUS and FRANC3D is shown in Fig. 5. FRANC3D uses the finite element method to calculate the mechanical parameters and simulate the growth of an arbitrary three-dimensional crack, while ABAQUS provides the initial finite element model and the operation solver, and FRANC3D is able to be used for inserting cracks, re-meshing and fatigue life calculation.

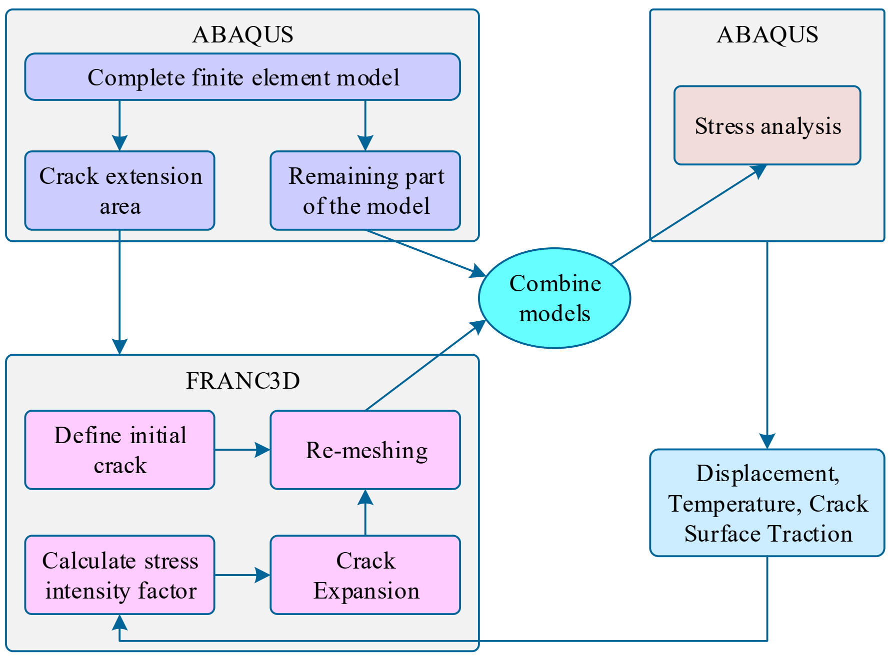

Fig. 5. Crack expansion joint simulation process

The natural gas pressure vessel has a large volume, and the crack defects are extremely small relative to the size of the whole model, the crack extension simulation using the traditional 1:1 scale model is difficult to calculate the magnitude of ordinary computers, and the simulation effect is difficult to intuitively display, so it is necessary to simplify the actual physical model. Due to the specificity of crack extension, just calculate the perimeter integral near the tip, the finite element model can be simplified to extract the crack defects near the block-like sheet. The natural gas pressure vessel is subjected to high internal pressure, so the problem of numerical simulation of surface cracks in the pressure vessel is simplified to the problem of combined tensile-flexural fatigue crack extension of a flat plate containing surface cracks.

Under the specified elliptical surface crack morphology, six groups of different initial crack depths and crack lengths are selected. The commonly used material for pressure vessel manufacturing, 16Mn, with a modulus of elasticity of $2.12*10^5$Mpa, is used. The surface crack is located in the center of the simulation model, and four groups of cracks with different initial short-axis-long-axis ratios (0.65, 0.75, 0.85, 0.95) are selected for comparative analyses. The bottom end was completely fixed, the pressure applied to the upper end surface of the model was 3Mpa, the pressure applied to the inner surface was 0.3Mpa, and the constant amplitude load stress ratio was 0.15.

3.3. Simulation of crack expansion rate

3.3.1. Initial Angle Crack Expansion. In order to obtain the effect of stress on crack extension, the extension study was carried out for cracks with and without stress loading, and the stress intensity factor at the leading edge of the crack and the crack extension distance were calculated. Extension studies were mainly carried out for cracks at two different locations, i.e., the initial crack was a 10 mm semicircular crack with an angle of 5° to the longitudinal section of the natural gas pressure vessel. As the crack expands, the crack extends to the outer surface where the inlet port intersects with the upper cylinder of the pressure vessel, and then the crack will continue to expand along both the upper cylinder and the inlet port of the pressure vessel, and the initial semi-circular crack gradually develops into a smooth circular shape as the crack continues to expand. Fig. 6 shows the crack expansion when the initial angle is 5°, where Fig. 6(a)~(b) shows the changes of crack stress intensity factor and expansion distance, respectively.

From the change of crack stress intensity factor, it can be seen that the stress intensity factor along path A under hydrostatic loading is larger than that along path A under stress-containing loading after the 10th step, and the stress intensity factor along path B under hydrostatic loading is larger than that along path B under stress-containing loading after the 50th step, but the difference of stress intensity factor is not large. Moreover, the stress intensity factor along path A under hydrostatic loading is larger than that along path B. After 30 steps, the stress intensity factor along path A under stress-containing load is larger than that along path B, and the difference increases as the crack continues to expand. The stress intensity factor under hydrostatic load only is greater than the stress intensity factor under stress load.

From the variation of crack extension distance, it can be seen that after the 25th step, the crack extension distance along path A under hydrostatic load is larger than the crack extension distance along path A under stress load, and after the 18th step, the crack extension distance along path B under hydrostatic load is larger than the crack extension distance along path B under stress load. After 35 steps, the stress intensity factor along path A is greater than that along path B under both loads, and the difference in stress intensity factor increases as the crack continues to expand. Therefore, the crack expansion rate along path A is greater than that along path B. The difference between the crack expansion distances under the two paths is getting larger and larger in the expansion process.

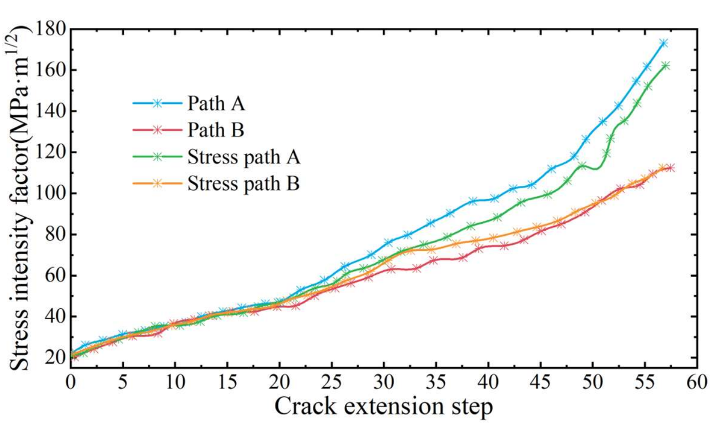

(a) Crack stress intensity factor

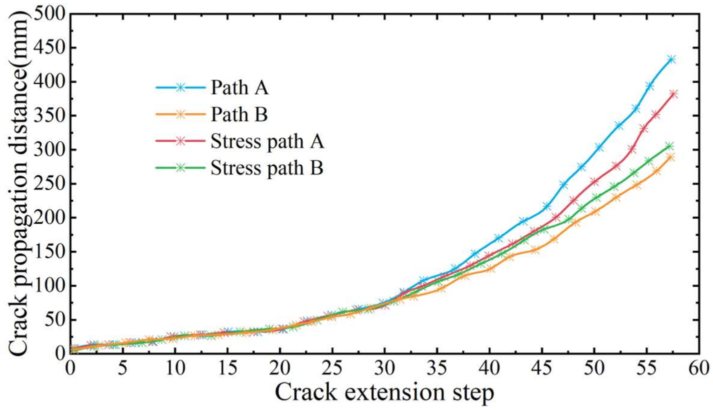

(b) Crack extension distance variation

Fig. 6. The initial Angle is the crack extension of the 5°

3.3.2. Analysis of crack extension pattern. The complexity and diversity of cracks in natural gas pressure vessels are the difficulties in calculating and analyzing the crack expansion rate. In this paper, simulations are carried out according to different initial crack profiles, and the initial crack profiles with short to long axis ratios of 0.65, 0.75, 0.85, and 0.95 are taken for the simulation of crack expansion, respectively. From the above analysis and simulation, the effect of initial shape on crack extension can be obtained. From the simulation results, the coordinates of the crack edge nodes can be extracted after crack expansion, so that the crack morphology after each expansion can be known. Taking the coordinates of the deepest part of the crack and the coordinates of the two points at the tip of the crack surface, it is possible to calculate the short-axis-long-axis ratio of the new crack edge with the approximate elliptical shape, and the crack extension data are organized to obtain the results shown in Tables 1 and 2.

Regardless of the crack expansion rate of the material, it is initially judged that the short to long axis ratio is between 0.814 and 1.00 in the steady state of crack expansion. By the value of crack extension rate, we can infer the steady state shape of crack extension, i.e., the short-long axis ratio tends to be 0.89. During the simulation process, the cracks with initial short-long axis ratios of 0.85 and 0.95 reach the steady state after crack extension. By theoretical calculation, the surface crack short-long axis ratio tends to 0.814 when the crack edge stress intensity factor is the same, i.e., the cracks with initial crack short-long axis ratios of 0.65 and 0.75 are simulated to be expanded for several times, so that the stress intensity factor of the crack edges reaches the steady state level.

Table 1. Crack propagation of short length axis ratio (mm)

Extended step	Short length axis ratio (0.95)			Short length axis ratio (0.85)		
	Cusp coordinates	Tip A	Tip B	Cusp coordinates	Tip A	Tip B
0	216	-4	4	218	-4	4
1	215.246	-4.326	4.326	217.814	-4.313	4.313
2	215.106	-4.751	4.751	217.537	-4.645	4.645
3	214.938	-5.062	5.062	217.238	-4.971	4.971
4	214.646	-5.384	5.384	216.843	-5.204	5.204
5	214.378	-5.691	5.691	216.574	-5.583	5.583
6	213.932	-6.017	6.017	216.184	-5.942	5.942
7	213.514	-6.428	6.428	215.895	-6.272	6.272
8	213.024	-6.884	6.884	215.603	-6.616	6.616
9	212.847	-7.064	7.064	215.294	-6.798	6.798

10	212.527	-7.435	7.435	215.016	-7.216	7.216
11	212.234	-7.871	7.871	214.834	-7.643	7.643
12	212.031	-8.114	8.114	214.572	-7.906	7.906
13	211.758	-8.423	8.423	214.303	-8.243	8.243
14	211.462	-8.596	8.596	214.002	-8.674	8.674
15	211.127	-9.173	9.173	213.884	-8.935	8.935
16	210.983	-9.545	9.545	213.607	-9.127	9.127
17	210.562	-9.968	9.968	213.292	-9.549	9.549
18	210.237	-10.212	10.212	213.028	-9.884	9.884
19	210.027	-10.507	10.507	212.875	-10.231	10.231
20	209.943	-10.985	10.985	212.463	-10.586	10.586

Table 2. Crack propagation of short length axis ratio (mm)

Extended step	Short length axis ratio (0.65)			Short length axis ratio (0.75)		
	Cusp coordinates	Tip A	Tip B	Cusp coordinates	Tip A	Tip B
0	218.5	-4	4	219	-4	4
1	218.127	-4.231	4.231	218.842	-4.102	4.102
2	217.956	-4.645	4.645	218.631	-4.493	4.493
3	217.563	-4.973	4.973	218.026	-4.841	4.841
4	217.024	-5.348	5.348	217.843	-5.065	5.065
5	216.837	-5.792	5.792	217.515	-5.337	5.337
6	216.526	-5.985	5.985	217.038	-5.795	5.795
7	216.131	-6.194	6.194	216.922	-6.043	6.043
8	215.945	-6.648	6.648	216.584	-6.187	6.187
9	-	-	-	216.101	-6.426	6.426
10	-	-	-	215.784	-6.841	6.841

Based on the crack extension morphology data in the above two tables about different fracture axis ratios, in order to observe the extension morphology change and the trend of short-long axis ratio at steady state more clearly, the length of crack extension in the depth direction of the pressure vessel is taken as the horizontal coordinate, and the short-long axis ratio of the crack morphology is taken as the vertical coordinate. The crack extension laws for different initial crack morphologies can be obtained as shown in Fig. 7.

The crack source with initial crack morphology of 0.95 and 0.85 tends to steady state after twenty times of expansion, and the short to long axis ratio of steady state tends to 0.9, this simulation confirms the existence of the steady state expansion of the crack and simulates the steady state value. There is an error of 1.11% with the theoretical value of 0.89 calculated from the theoretical derivation, which may be due to the error in the calculation of the slope in the theoretical calculation, and the error in the determination of the coordinate points in the simulation process. The crack initial morphology short-long axis ratio of 0.75, 0.65 of the crack source expansion process, the short-long axis ratio changes faster, which is basically consistent with the theoretical calculation value.

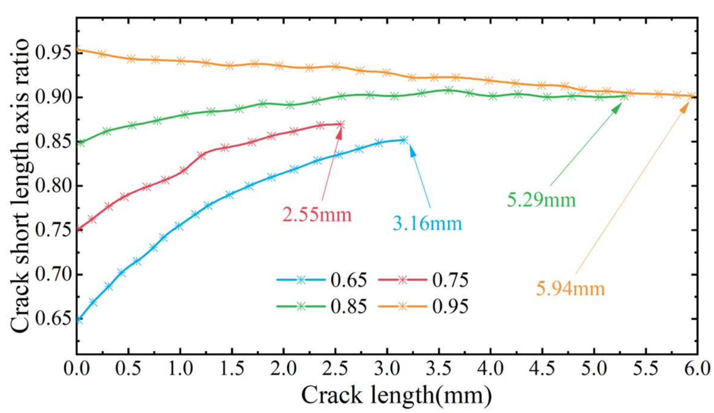

Fig. 7. Pattern of crack propagation

3.3.3. Analysis of the effects of stress ratios. Natural gas pressure vessels are subjected to a variety of different loads in the course of use, and the crack expansion rate of the vessel is different under different loads, and the crack expansion rate provides an important basis for the estimation of crack life, so it is important to study the crack expansion rate of the pressure vessel cracks under different loads. In this section, the amplitude of the stress intensity factor of the natural gas pressure vessel is changed by modeling different stress ratios, so as to simulate the different loading environments in the actual working conditions. According to the Paris formula, when the magnitude of the stress intensity factor is changed, the crack expansion rate is also changed. In this section, the crack extension rate is calculated for different stress ratios of 0.15, 0.35, and 0.55, and the variation curves between crack length and extension rate are plotted as shown in Fig. 8.

When the stress ratio is larger, the crack extension rate increases faster. When the crack of the pressure vessel extends to the vicinity of 20 mm, the crack extension rate starts to decrease sharply, which is due to the contact between the two material surfaces in the establishment of the model for the ideal type of contact, when the crack extends to the metal bonding surface, the interface of the material has an inhibiting effect on the extension rate of the crack, which reduces the extension rate of the crack. When the crack continues to expand through the interface to the cladding metal, the expansion rate is restored. When the stress is relatively large, the crack expansion rate is significantly larger than the expansion rate when the stress is relatively small. Therefore, in practice, natural gas pressure vessels should be avoided under such conditions, which can improve the service life of natural gas pressure vessels.

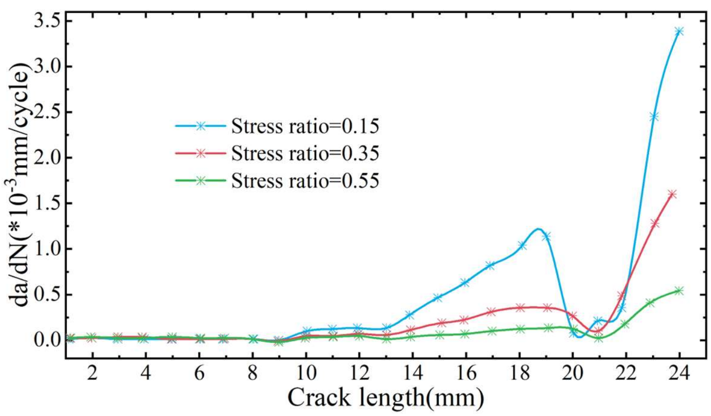

Fig. 8. The effect of stress on crack expansion rate

4. Yield strength dependence of natural gas pressure vessels

Pressure vessels are commonly used equipment in the natural gas field, according to relevant statistics, the natural gas industry due to corrosion of pressure piping and vessel equipment caused by safety accidents accounted for the majority of all accidents. Pressure vessels are generally made of metal, and they are prone to corrosion in the high-pressure or corrosive environment of natural gas for a long period of time, which in turn leads to uneven stress distribution in the pressure vessel and destruction of metal materials. Therefore, to do a good job of natural gas pressure vessel yield strength dependence analysis work, to explore the causes of natural gas pressure vessel deformation, can provide reliable data support for the proposed targeted preventive measures.

4.1. Fatigue modeling of pressure vessel steels

4.1.1. Elastic-viscoplastic intrinsic modeling. Elasto-viscoplastic mechanics focuses on the mechanical behavior of materials credited with an elastic deformation history that takes into account the transient and viscous effects of the material during plastic deformation. The visco-plastic strain deflection tensor is usually denoted by $\varepsilon_{ij}^{\eta p}$ [28].

Malvern, on the basis of considering the physical relationship between elasticity and strain rate effects in materials, proposed that the total strain rate $\{\dot{\varepsilon}\}$ is equal to the sum of the elastic strain rate $\{\dot{\varepsilon}^{e}\}$ and the viscoplastic strain rate $\{\dot{\varepsilon}^{vp}\}$, i.e.:

$$\{\dot{\varepsilon}\} = \{\dot{\varepsilon}^{e}\} + \{\dot{\varepsilon}^{\eta p}\} \tag{36}$$

where the "·" above the letter represents the differentiation with respect to time, and the elastic strain rate can be written directly:

$$\{\dot{\varepsilon}^{e}\} = [D]^{-1}\{\dot{\sigma}\} = \frac{1}{2G}\{\dot{S}\} \tag{37}$$

where $\{D\}$ is the elastic matrix, $\{\dot{\sigma}\}$ is the rate of change of total stress, $\{\dot{S}\}$ is the rate of change of stress bias invariance, and G is the elastic shear modulus.

Elasto-viscoplastic materials do not take into account the viscosity of the elastic deformation stage, and the initial yield criterion is consistent with that in the non-viscoplastic theory, and under isotropic hardening conditions, the loading surface in the stress space is just a similar enlargement of the initial yield surface, viz:

$$F\left(\sigma_{ij}, \dot{\varepsilon}^{\eta p}\right) - F_0 = 0 \tag{38}$$

For elasto-viscoplastic materials, during elastic deformation, the strain rate is proportional to the differential of the stress bias with respect to time and the scaling factor is a constant; during the viscoplastic stage of deformation, the strain rate is proportional to the stress bias but the scaling factor is a nonconstant term containing a viscosity and relating $\sqrt{J_2'}$.

The yield surface $F=0$ is assumed to be regular and at the same time externally convex in the stress space. He proposed the following relationship between the viscoplastic strain rate $\dot{\varepsilon}^{\eta p}$ and the instantaneous stress:

$$\dot{\varepsilon}^{\eta p} = \gamma < \phi(F) > \frac{\partial Q}{\partial \sigma_{ij}} \tag{39}$$

where Q is the plastic potential function and γ is the plastic flow parameter. Then $\phi(F)$ can be expressed as:

$$\langle \phi(F) \rangle = \begin{cases} 0 & Which\ F \le 0 \\ \phi(F) & Which\ F > 0 \end{cases} \tag{40}$$

For the viscoplastic strain rate, when the correlation flow assumption is used, i.e., the yield function and the plastic flow potential function of the concrete material are the same, the viscoplastic strain rate can be defined as:

$$\dot{\varepsilon}^{\eta p} = \gamma < \phi(F) > \frac{\partial F}{\partial \sigma_{ij}} \tag{41}$$

where F is the loading function. In this paper, we refer to the existing relevant literature taken as:

$$\phi(F) = \left(\frac{F - F_0}{F_0}\right)^{N} \tag{42}$$

where N is the material constant and F_0 is the one-way yield stress.

Substituting Eqs. (37), (40)~(42) into Eq. (36) yields the elasto-viscoplastic isomorphic model of the associated flow law in the general state of stress, viz:

$$\begin{cases} \{\dot{\varepsilon}\} = \dfrac{1}{2G}\{\dot{S}\} & F \le 0 \\ \{\dot{\varepsilon}\} = \dfrac{1}{2G}\{\dot{S}\} + \gamma\left(\dfrac{F - F_0}{F_0}\right)^N \dfrac{\partial f}{\partial\{\sigma\}} & F > 0 \end{cases} \tag{43}$$

4.1.2. Realization of the intrinsic model. The widely used ABAQUS solver is used as an example to illustrate how the viscoplastic eigenstructure model can be implemented with finite element software through UMAT, the interface subroutine of ABAQUS that defines the material eigenstructure relationship. When using ABAQUS software, the Cauchy stress tensor must be used in the constitutive equations.ABAQUS solves the nonlinear finite element equilibrium equations using the Newton-Raphson method for the quasi-static loading case, with:

$$\sum\left(\int B^{\tau} JBdV\right)C^k = P(t+\Delta t) - \sum\int B^T\left[\sigma(t) + \Delta\sigma\left(\Delta u^k\right)\right]dV \tag{44}$$

$$\Delta u^{k+1} = \Delta u^k + C^k \tag{45}$$

where matrix B converts node displacement increments into strain increments by the following equation, viz:

$$\Delta\varepsilon = B \cdot \Delta u \tag{46}$$

The constant stiffness method is one of the simplest solution methods. For nonlinear problems, it can always be expressed for one degree of freedom when solving the problem in finite elements as:

$$H\varphi + f = 0 \tag{47}$$

where φ is the basic unknown vector. If it is a linear problem, H is not related to φ, and φ is a primary term, so it is clearly a linear equation. If H is related to φ, multiple terms appear in φ of the equation and it becomes a nonlinear problem. To obtain the most fundamental unknowns, it is necessary to solve the system of nonlinear equations. For the constant stiffness method, φ from the previous iteration step is used to solve H for the current iteration step, and then f and H are used in the following equation to solve the current φ:

$$\varphi_{n+1} = -H\left(\varphi_n\right)^{-1} f \tag{48}$$

From the above equation, it is known that the constant stiffness method first requires an initial value of φ_0 in order to start the iteration. In addition, the inverse of H is required for each solution, or the inverse of the stiffness matrix if a system of nonlinear equations is being solved. In this method, when the difference between φ_n and φ_{n+1} is very small for two times before and after the solution process, the solution is considered to be close to the true value and the iteration ends.

In this example, numerical simulation of natural gas pressure vessel is carried out by using the material parameters of natural gas pressure vessel in the general case, and the specific steps are as follows:

1) Create a 1:1 scale model of the test piece in the geometric model modeling module of ABAQUS software.

2) Based on the implementation of the intrinsic model in the software, customize the user material in the attribute module.

3) In the analysis step module, adopt the initial analysis step and static common subsequent analysis step mode.

4) In the load constraint module, in order to make the numerical simulation process more in line with the actual test process, a solid support constraint is applied to one end of the geometric model

and a displacement constraint is applied to the other end to represent the force state of the test piece, and for the uniaxial tensile test, a displacement load of 10% is applied to the geometric model.

5) In the meshing module, the 3D model with C4D5 cells is used for free meshing of the entity with finite elements, and the mesh is subdivided for the scaled section of the uniaxial tensile test piece, with the total number of cells being 1842 and the total number of nodes being 2368.

6) Submit the job and enter the post-processing module after getting the structure.

4.2. Fatigue Yield Strength of Pressure Vessel Steels

4.2.1. Effect of loading rate. The hysteresis curves of different stages of natural gas pressure vessel steel fatigue under cyclic loading with strain rates of $0.001s^{-1}$, $0.006s^{-1}$, $0.012s^{-1}$ and strain amplitude of 0.6% are shown in Fig. 9. Among them, Fig. 9(a)~(c) shows the stress-strain hysteresis curves of the initial stage, stabilization stage and fracture stage, respectively.

It can be seen that the change in the loading rate has an effect on the cyclic stress-strain relationship for the fatigue of natural gas pressure vessel steels. From the figure, it can be seen that with the increase of strain rate, the cyclic hysteresis curves have obvious morphological differences, the two higher loading rates have a certain strengthening effect on the material, which is reflected in the curve morphology is a smaller range of plastic strain and a larger range of stress. Compared to the loading strain rate of $0.001s^{-1}$, the initial cyclic stress range and steady state cyclic stress range of the material at both loading rates of $0.006s^{-1}$ and $0.012s^{-1}$ gradually increase, while the stress range at the loading rate of $0.012s^{-1}$ decreases in comparison to that at the loading rate of $0.006s^{-1}$.

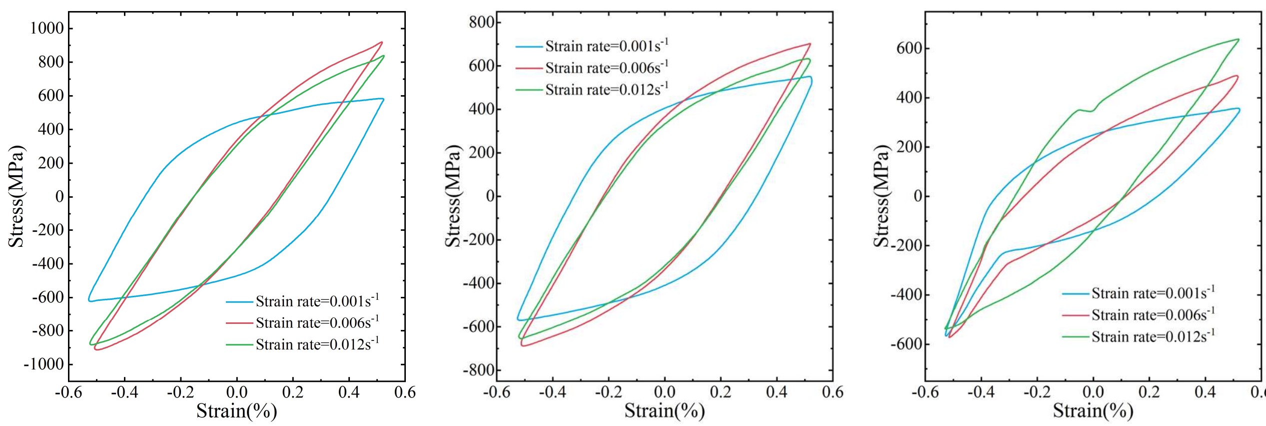

(a) Initial stage (b) Stable phase (c) Fracture stage

Fig. 9. The hysteresis curve of different stages

Figure 10 shows the cyclic response behavior of the material at different loading rates. From the figure, it can be seen that at two higher strain rates ($0.006s^{-1}$ and $0.012s^{-1}$), the material shows cyclic softening phenomenon, and the degree of softening is basically the same, and the number of cycles to reach cyclic stability is also basically the same. There is no obvious cyclic softening characteristic of the material at the loading rate of $0.001s^{-1}$, which is closer to the cyclic response at the strain amplitude of 0.2%. In addition, the number of fracture cycles increased significantly when the loading rate was increased from $0.001s^{-1}$ to $0.006s^{-1}$, and decreased when the loading rate was increased from $0.006s^{-1}$ to $0.012s^{-1}$.

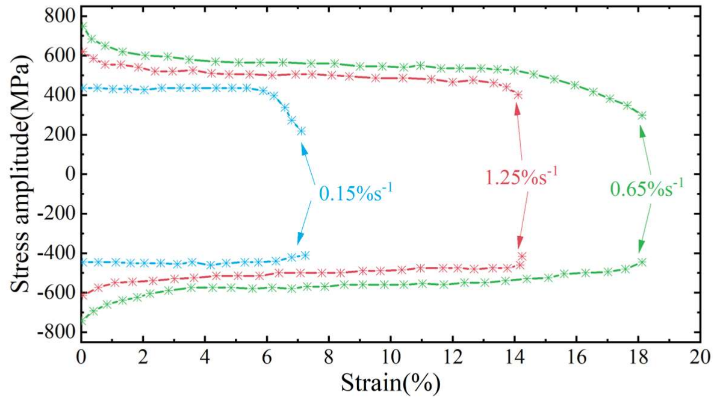

Fig. 10. Cyclic stress response curve

In low-cycle fatigue testing, due to the relatively large loads applied to the material (often reaching or even exceeding the yield stress of the material), the material has large plastic deformations and localized damage under loading. Generally speaking, the loading rate is low, so the single cycle time is relatively long, which makes the tensile stress that can drive crack nucleation and crack extension act on the material for a longer period of time, so that the material under cyclic loading plastic deformation is more adequate, and the damage of the material is more serious, resulting in a reduction of the fatigue life of the material. With the increase of loading rate, the single cycle time becomes shorter, and the fatigue life is improved to a certain extent, but when the loading rate reaches a certain value, the internal structure of the material will produce strong internal friction, resulting in the local temperature of the material increases, fatigue crack nucleation and crack extension accelerated, shortening the fatigue life of the material.

4.2.2. Mechanical properties after elevated temperatures. Yield strength is a metal material yield phenomenon occurs when the yield limit, if the material or component encountered greater than this limit of external load, will produce unrecoverable plastic deformation, so the yield strength is an important mechanical properties of steel index. When the natural gas pressure vessel steel in the high temperature cooling there is still a clear yield platform, the yield strength at this time yield strength to take the lower limit of the yield platform as the yield strength value of steel. Part of the specimen cooled by immersion above 600℃, its stress-strain curve does not exist obvious yielding stage, according to the European norms, take the stress value corresponding to 0.25% of the residual strain as its yield strength value. Based on this, this paper simulates the change of yield strength of natural gas pressure vessel steels at different temperatures through different cooling methods, and the specific results are shown in Fig. 11, where Fig. 11(a)~(b) shows the yield strength and ultimate strength, respectively.

For the three different cooling methods, when the high temperature is less than or equal to 400 ℃, the change value of yield strength are very limited, and the deviation value of yield strength at room temperature is not more than 2.5%, which indicates that when the temperature is below 400 ℃, the change value of cooling method on the yield strength of natural gas pressure vessel steel can be basically ignored. However, when the temperature rises to 500 ℃, the strength value of the specimen with natural cooling and foam cooling shows a substantial decrease, and with the increase in temperature, the decrease in yield strength value also shows a trend of growth, for example, at 500 ℃, the yield strength of the specimen with natural cooling is 353.27 MPa, when the temperature comes to 900 ℃, the yield strength of the natural gas pressure vessel steel value is only 280.42 MPa, the same phenomenon also occurs in the specimen cooled by foam extinguishing agent. The same phenomenon also occurred in the specimens cooled by foam extinguishing agent. It shows that the higher temperature has a greater effect on the yield strength of natural gas pressure vessel steel.

Comparatively, the yield strength of the immersion-cooled specimen is completely different, when the temperature is set to 900 ℃, its yield strength value even compared with the room temperature (452 MPa) increased by 4.76%, which is due to the immersion cooling is equivalent to the steel quenching, the most direct effect is to make the strength of the steel increased, toughness decreased. In addition, when the temperature is less than or equal to 400°C, the change in ultimate strength fluctuates only within the range of ±2.4%, indicating that when the value of the temperature is not more than 400°C, the change in the cooling method will not affect the value of the ultimate strength of the steel of the natural gas pressure vessel. When the temperature reaches 500℃, the change trend of ultimate strength of specimens with natural cooling and foam cooling is similar to that of yield strength, and numerically, the ultimate strength of specimens with natural cooling and specimens with foam cooling at 900℃ are 423.69MPa and 434.29MPa, respectively, which indicates that the higher the temperature, the greater the influence on the ultimate strength of steel for natural gas pressure vessels when the temperature is above 500℃; The ultimate strength of specimens cooled by immersion water has a significant increase after 900 ℃, its ultimate strength value even increased by 28.22% compared with the room temperature (551), which is 7.23 times the increment of the yield strength value. Therefore, the yield strength of natural gas pressure vessels is significantly affected by temperature, and changes in temperature can cause the yield strength of natural gas pressure vessels to change to a greater extent.

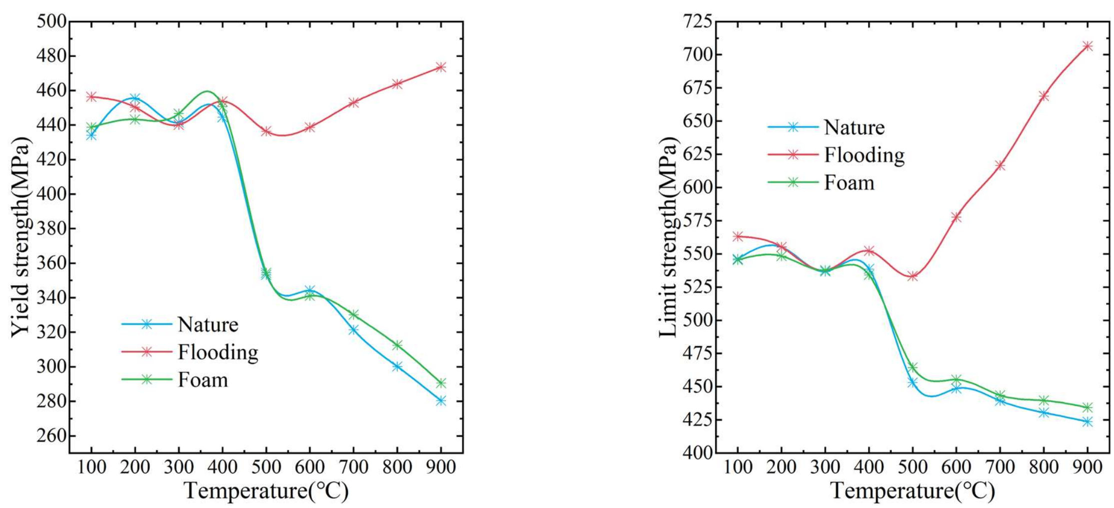

(a) Yield strength (b) Limit strength

Fig. 11. Yield strength and limit strength

5. Conclusion

In this paper, the fatigue performance, crack extension efficiency, and yield strength dependence of natural gas pressure vessel steels are explored based on stress-strain, stress-strength, and elastic-viscoplastic intrinsic models in combination with ABAQUS and FTANC3D simulation software. Based on the simulation results, it can be seen that the fatigue limit of the specimen in the air environment is 323.78MPa in 10^7 cycles, while there is no fatigue limit in the corrosion environment in the 10^7 cycles. Regardless of the crack extension rate of the material, it is initially determined that the short-long axis ratio at steady state of crack extension is between 0.814 and 1.00. When the crack in the pressure vessel extends to the vicinity of 20 mm, a sharp decrease in the crack extension rate begins to occur. The yield strength of the naturally cooled specimen at 500°C was 353.27 MPa, and when the temperature came to 900°C the yield strength value of the natural gas pressure vessel steel was only

280.42 MPa. The safety of natural gas pressure vessels can be better ensured by analyzing the steel fatigue properties, crack extension efficiency and yield strength of natural gas pressure vessels.

Funding

This work was supported by Scientific Research Program Funded by Education Department of Shaanxi Provincial Government (Program No. 22JK0326) and Shaanxi Province's Key Research and Development Program (General Projects) (Program No. 2024GX-YBXM-253) and School-level Research Projects of Shaanxi Energy Institute of Technology (Program No. 2021QN04).

References

[1] Makarova, I., Shubenkova, K., & Sadygova, G. (2018). Compressed natural gas as motor fuel: possibilities, problems and solutions. Archiwum Motoryzacji, 82(4), 43-62.

[2] Elkafas, A. G., Khalil, M., Shouman, M. R., & Elgohary, M. M. (2021). Environmental protection and energy efficiency improvement by using natural gas fuel in maritime transportation. Environmental Science and Pollution Research, 28(43), 60585-60596.

[3] Mayrhofer, M., Koller, M., Seemann, P., Prieler, R., & Hochenauer, C. (2021). Assessment of natural gas/hydrogen blends as an alternative fuel for industrial heat treatment furnaces. International journal of hydrogen energy, 46(41), 21672-21686.

[4] Xuedong, C., Zhichao, F., Jie, D., Zhibin, A., & Mingdong, H. (2020, August). Safety assessment of pressure vessels in service for more than 20 years. In Pressure Vessels and Piping Conference (Vol. 83815, p. V001T01A084). American Society of Mechanical Engineers.

[5] Mali, M. A., Bhosale, M. H., Bedi, M. D. S., & Modasara, M. A. (2017). A review paper on study of pressure vessel, design and analysis. Int. Res. J. Eng. Technol, 4, 1369-1374.

[6] Jegatheesan, J., & Zakaria, Z. (2018). Stress analysis on pressure vessel. Environ. Ecosyst. Sci, 2, 53-57.

[7] Xiao, B., Yang, B., Xuan, F. Z., Wan, Y., Hu, C., Jin, P., ... & Yang, K. (2019). In-situ monitoring of a filament wound pressure vessel by the MWCNT sensor under hydraulic fatigue cycling and pressurization. Sensors, 19(6), 1396.

[8] Niu, X. P., Zhu, S. P., He, J. C., Ai, Y., Shi, K., & Zhang, L. (2021). Fatigue reliability design and assessment of reactor pressure vessel structures: Concepts and validation. International Journal of Fatigue, 153, 106524.

[9] Kim, E. S. (2019). A study on fatigue life evaluation of pressure vessel made of ASME SA240-316L material using numerical analysis. Applied Mechanics and Materials, 893, 1-5.

[10] Puryear, J., Ramirez, G., Botard, C., & Kenady, K. (2018). Fracture toughness and brittle failure: A pressure vessel case study. Process Safety Progress, 37(2), 305-310.

[11] Das, A. (2017). Fracture complexity of pressure vessel steels. Philosophical Magazine, 97(33), 3084-3141.

[12] Mathew, N. M., Vishnuvardhan, S., Raghava, G., & Santhi, A. S. (2017). Corrosion fatigue crack growth studies on pressure vessel and piping steels in water environment. Archives of Metallurgy and Materials, 62.

[13] Shen, W., & Zhao, Y. P. (2017). Quasi-static crack growth under symmetrical loads in hydraulic fracturing. Journal of Applied Mechanics, 84(8), 081009.

[14] Li, D., Huang, P., Guo, X., Zheng, X., Lin, J., & Chen, Z. (2018). Fatigue crack propagation behavior of RC beams strengthened with CFRP under cyclic bending loads. Fatigue & Fracture of Engineering Materials & Structures, 41(1), 212-222.

[15] Ma, Y., He, S., Song, D., He, X., Chen, T., Shen, F., ... & Wang, J. (2024). Crack propagation characteristics and fatigue life of the large austenitic stainless steel hydrogen storage pressure vessel. International Journal of Pressure Vessels and Piping, 210, 105226.

[16] Lou, X., Pathania, R., & Andresen, P. L. (2017). Effects of chloride transients on stress corrosion crack in pressure vessel low alloy steels in high temperature water. Corrosion Science, 126, 305-316.

[17] Zhou, X., He, R., Zhou, T., & Liu, Z. (2022). Crack propagation on the surface of the bottleneck of a pressure vessel considering the initial crack angle. Applied Sciences, 12(8), 3913.

[18] Amsterdam, E., Wiegman, J. W. E., Nawijn, M., & De Hosson, J. T. M. (2022). The effect of crack length and maximum stress on the fatigue crack growth rates of engineering alloys. International Journal of Fatigue, 161, 106919.

[19] Okazaki, S., Wada, K., Matsunaga, H., & Endo, M. (2017). The influence of static crack-opening stress on the threshold level for shear-mode fatigue crack growth in bearing steels. Engineering Fracture Mechanics, 174, 127-138.

[20] Main, B., Jones, M., & Barter, S. (2021). The practical need for short fatigue crack growth rate models. International Journal of Fatigue, 142, 105980.

[21] Scales, M., Anderson, J., Kornuta, J. A., Switzner, N., Gonzalez, R., & Veloo, P. (2022). Accurate estimation of yield strength and ultimate tensile strength through instrumented indentation testing and chemical composition testing. Materials, 15(3), 832.

[22] Paul, S. K. (2020). Correlation between endurance limit and cyclic yield stress determined from low cycle fatigue test. Materialia, 11, 100695.

[23] Bi, Y., Yuan, X., Lv, J., Bashir, R., Wang, S., & Xue, H. (2021). Effect of yield strength distribution welded joint on crack propagation path and crack mechanical tip field. Materials, 14(17), 4947.

[24] Songjiang Lu. (2025). Extracting mechanical properties and uniaxial stress-strain relation of materials from dual conical indentation by machine learning. European Journal of Mechanics / A Solids105598-105598.

[25] Caibao Liu,Zhen Lu,Yuanqing Wang & Xiongyan Li. (2025). Research on bearing capacity of four-member spatial tubular X-joints. Journal of Constructional Steel Research109395-109395.

[26] Wei Gao,Shou Yuan,Shuangshuang Ge,Zhihao Zhao & Yi Han. (2025). Theoretical study on the stress intensity factor at the crack tip of a water-bearing rock. Applied Mathematical Modelling115976-115976.

[27] Xinru Zhao,Shulan Liu,Zun Xie,Zhao Liu,Dianwu Wang & Lingen Luo. (2025). Effects of temperature and strain rate on crack propagation in NiCoCr multi-principal element alloys: A molecular dynamics simulation. Materials Today Communications111667-111667.

[28] Xiaojuan Shu,Zhichao Wang,Yiqin Peng,Ziwei Zhou & Yinghui Tian. (2024). A novel elasto-viscoplastic constitutive model for predicting the embankment settlement on soft structured clay. Computers and Geotechnics106093-.